Journal of Intelligent and Robotic Systems **25:** 227–254, 1999.

On the Robust Nonlinear Motion Position and Force Control of Flexible Joints Robot Manipulators

ATEF T. MASSOUD
Mechanical Design and Production Department, Cairo University, Giza, Egypt 12316; e-mail: atefma@cairo.eun.eg

HODA A. ELMARAGHY
Intelligent Manufacturing Systems Center, University of Windsor, Ontario, Canada N9B 3P4; e-mail: hae@ims.uwindsor.ca

TAREK LAHDHIRI
General Motors, VSAS Process Center Warren, MI 48092; e-mail: tl007@ieee.org

(Received: 14 October 1997; in final form: 22 February 1999)

Abstract. The design of a robust nonlinear position and force controller for a flexible joints robot manipulator interacting with a rigid environment is presented. The controller is designed using the concept of feedback linearization, sliding mode techniques, and LQE estimation methodologies. It is shown that the nonlinear robot manipulator model is feedback linearizable. A robust performance of the proposed control approach is achieved by accounting for the system parameters uncertainties in the derivation of the nonlinear control law. An upper bound of the error introduced by parametric uncertainties in the system is computed. Then, the feedback linearizing control law is modified by adding a switching action to compensate the errors and to guarantee the achievement of the desired tracking performance. The relationship between the minimum achievable boundary layer thickness and the parametric uncertainties is derived. The proposed controller is tested using an experimental flexible joints robot manipulator, and the results demonstrate its potential benefits in reducing the number of sensors required and the complexity of the design. This is achieved by eliminating the need for nonlinear observers. A robust performance is obtained with minimum control effort by taking into account the effect of system parameter uncertainties and measurement noise.

Key words: robotics, flexible joints, feedback linearization, sliding mode control, LQE techniques.

1. Introduction

In many robot manipulator systems, the joint flexibility, introduced by the drive systems, such as shafts, belts, and chains, cannot be neglected [1, 2]. Poorly damped oscillations may take place whenever the joint resonant frequencies are excited which are usually located within the control bandwidth. Joint's flexibility may degrade the controller performance and may cause unstable behavior. Therefore, joint's flexibility has to be considered in the control design in order to achieve the desired system performance.

In several industrial applications, the robot end effector comes into contact with the environment. Therefore, there is a need to control both the position and force at the end effector in order to execute contact tasks properly. This problem has been extensively studied for rigid robot manipulators. When the robot motion is constrained by perfectly rigid surfaces, there are kinematic constraints on the motion of the end effector. McClamroch and Wang [3], Mills and Goldenberg [4], and Yoshikawa [5, 6] considered these constraints in the dynamic model and in the derivation of the control law. However, in the force control approaches by Khatib [7] and DeLuca et al. [8], the constraints were not considered for decoupling, whereas the dynamic interactions were.

From this brief discussion, it can be seen that there is a need to consider joint flexibility in modelling and control [1, 2] and to control both position and force of the robot end point. Also, it is important to note that the joint flexibility has to be accounted for, more in the case of force control than for pure position control [9, 10]. However, the problem of controlling both position and force of flexible joints robot manipulators did not receive much attention by the control and robot theorists and few solutions have been reported in the literature. Krishnan and McClamroch [11] applied a linear quadratic controller for the linearized constrained model. Mills [12] applied the idea of a composite control to a singular perturbed model. Spong [13] utilized the concept of integral manifold and corrective control of singularly perturbed nonlinear systems to extend the force control of rigid robots to the case of flexible joints. Jankowski and ElMaraghy [14] used the generalized coordinate portioning technique for coordinate reduction which ensures exact feedback linearization for hybrid position and force control.

Researchers proposed some adaptive control strategies for position control of flexible joint robot manipulators. Ghorbel et al. [15] and Hung [16] applied the adaptive control algorithm developed by Slotine and Li [17] to flexible joint robots. They simply modified the control law derived for rigid robots by adding a corrective term to damp out the elastic oscillations at the joints. The results were applied to an experimental single-link flexible-joint robot. The variable structure control approach was adopted by Sira-Ramiraz et al. [18] in the design of the outer loop control law for the linearized system. The system was first linearized by the nonlinear feedback and coordinate transformation. The availability of the state vector of the linearized model is assumed when designing the robust controller. Mrad and Ahmad [19] derived an adaptive control law based on an energy-motivated Lyapunov function and a linear parametrization model of the links system only. Recently, ElMaraghy and Massoud [20] presented a model-based adaptive algorithms using inverse dynamics techniques and dynamic decoupling. These algorithms were implemented using an experimental manipulator and very promising results were obtained.

The previously discussed control approaches for force and position control of flexible-joint robots suffer from some limitations. First, none of these approaches was experimentally tested except the one presented in [20]. Second, most of the

controller design use the singular perturbation techniques. This method is computationally expensive, and since it is interactive, it makes it impossible to symbolically formulate the equations of motion [14]. Third, the problem of system parameters uncertainties was not considered in most of the existing controllers. Since such parameters cannot be known exactly, then any realistic control design should account for these uncertainties. Fourth, the need for measuring the full transformed state vector is a problem common to all feedback linearization or inverse dynamics based-controllers. Some of these control designs assume that all states are available. However, this assumption may not hold true and, in general, an observer is needed to provide an estimate of the state. Existing observer designs range from sliding mode to nonlinear adaptive observers. However, the design of nonlinear observers is generally very complex and defeats the whole purpose of using feedback linearization, since the control design problem becomes nonlinear. In addition, most of the existing controller designs assume only noise-free measurements. This is often not true and, hence, noise must be taken into account.

The objective of this paper is to present a robust nonlinear position tracking and force controller for a two-link flexible joint robot manipulator. The controller is designed using the concept of exact feedback linearization [21], sliding mode control techniques, and linear optimal estimation techniques (LQE) [22]. The proposed control approach takes into consideration the joint flexibility, the system parameter uncertainties and measurement noise in order to achieve robust performance and robust stability. In addition, the number of required measurement sensors is reduced. The proposed control approach requires measurements of only the joint angular positions and velocities.

This paper is organized as follows: Section 2 presents the robot manipulator model, Section 3 contains the derivation of the linearizing state transformation using the concept of feedback linearization. Section 4 presents the constraint frame and force decoupling, Section 5 contains the design of the robust sliding mode controller, Section 6 discusses the experimental results, and Section 7 contains conclusions and plans for the future.

2. Dynamic Model of a Two-Link Flexible Joint Robot Manipulator

Consider the two-link flexible joint robot manipulator of Figure 1. The equations of motion of a two-degree of freedom flexible joint manipulator in the presence of contact forces, are given by (see [23])

$$D(q)\ddot{q} + C(q, \dot{q}) + B_l\dot{q} - K(q_m - q) = -J^{\mathrm{T}}F, \tag{1}$$

$$I_m\ddot{q}_m + B_m\dot{q}_m + K(q_m - q) = \tau, \tag{2}$$

where q is the link angular vector, q_m is the motor angular position vector, $D(\cdot)$ is the manipulator inertia matrix, $C(\cdot)$ is the Coriolis and centrifugal force vector, K is the joint stiffness matrix, I_m is the rotor inertia matrix, B_m is the motor

viscous friction matrix, B_l is the joints viscous friction matrix, J is the manipulator Jacobian, F is the force vector at the end effector expressed in the reference frame, and τ is the control torque input. In (1)–(2), the expressions of the different system variables and parameters are given by

$$\begin{aligned} q &= [q_1 \quad q_2]^{\mathrm{T}}, \qquad q_m = [q_{m_1} \quad q_{m_2}]^{\mathrm{T}}, \\ F &= [F_x \quad F_y]^{\mathrm{T}}, \qquad \tau = [\tau_1 \quad \tau_2]^{\mathrm{T}}, \end{aligned} \tag{3}$$

$$C(q,\dot{q}) = d_3\dot{q}_2 \sin q_2[-(2\dot{q}_1 + \dot{q}_2)] \quad \dot{q}_2]^{\mathrm{T}}, \tag{4}$$

$$D(q) = \begin{bmatrix} d_1 + 2d_2\cos q_2 & d_3 + d_2\cos q_2 \\ d_3 + d_2\cos q_2 & d_3 \end{bmatrix}, \tag{5}$$

$$J(q) = \begin{bmatrix} -l_1\sin q_1 - l_2\sin(q_1+q_2) & -l_2\sin(q_1+q_2) \\ l_1\cos q_1 + l_2\cos(q_1+q_2) & l_2\cos(q_1+q_2) \end{bmatrix}, \tag{6}$$

$$\begin{aligned} K &= \begin{bmatrix} k_1 & 0 \\ 0 & k_2 \end{bmatrix}, \qquad B_l = \begin{bmatrix} b_{l_1} & 0 \\ 0 & b_{l_2} \end{bmatrix}, \\ B_m &= \begin{bmatrix} b_{m_1} & 0 \\ 0 & b_{m_2} \end{bmatrix}, \qquad I_m = \begin{bmatrix} I_{m_1} & 0 \\ 0 & I_{m_2} \end{bmatrix}, \end{aligned} \tag{7}$$

$$\begin{aligned} d_1 &= I_1 + I_2 + m_1a_1^2 + m_2\left(l_1^2 + a_2^2\right) + m_{r_2}l_1^2, \\ d_2 &= m_2l_1a_2, \\ d_3 &= I_2 + m_2a_2^2. \end{aligned} \tag{8}$$

In Equation (8), $I_i,\ m_i,\ a_i$, and l_i are, respectively, the moment of inertia about an axis parallel to the axis of rotation passing through the center of mass, the mass, the distance from the center of rotation to the center of mass, and the length of link $i,\ i = 1, 2$, while m_{r_2} is the mass of the second motor's rotor. Computing the determinant of the manipulator inertia matrix $D(\cdot)$ yields

$$\begin{aligned} \gamma(q_2) &\triangleq \det(D(q)) \\ &\geqslant \left(I_2 + m_2a_2^2\right)\left(I_1 + m_1a_1^2 + m_{r_2}l_1^2\right) + I_2m_2l_1^2 > 0, \quad \forall q_2 \in \mathbb{R}. \end{aligned} \tag{9}$$

Using Equation (9), the system dynamics (1)–(2) can be rewritten in a state space form as

$$\dot{Y} = A_1(Y) + \sum_{i=1}^{m} b_iu_i + A_2(Y)F, \quad m = 2, \tag{10}$$

where $A_1(Y),\ b_1,\ b_2$, and $A_2(Y)$ are defined accordingly whereas the state vector Y and the control inputs u_1 and u_2 are given by

$$\begin{aligned} Y &= [y_1 \ \ldots \ y_8]^{\mathrm{T}} = [q_1\ q_2\ q_{m_1}\ \dot{q}_1\ \dot{q}_2\ \dot{q}_{m_1}\ \dot{q}_{m_2}]^{\mathrm{T}}, \\ u_1 &= \tau_1, \qquad u_2 = \tau_2. \end{aligned} \tag{11}$$

Note that in this paper, we consider only such planar motions where gravity force does not occur. The model (10)–(11) is a comprehensive model that has the advantage of capturing the essential system dynamics while reducing the complexity of the controller design. Next, the concept of MIMO feedback linearization is used to design a nonlinear position/force controller for the nonlinear system (10).

3. Application of the Concept of FL To The Two-Link Flexible Joint Robot Manipulator System

In the design of feedback control laws for complex nonlinear systems, the concept of feedback linearization has emerged as a promising technique. The problem of feedback linearization can be formulated as follows: Given a nonlinear system of the form of (10) with a stable equilibrium point X^0, find if possible, a $\mathcal{C}^\infty$-one-to-one transformation $T(X)$ and an appropriate control law, both defined in an open and dense set W_Y, such that the dynamics of the transformed system has the form of

$$\dot{Z} = \Lambda Z + B\nu, \tag{12}$$

where Λ and B are constant matrices with the pair (Λ, B) being controllable. Necessary and sufficient conditions for the existence of such a transformation are stated by the following theorem.

THEOREM 1 ([21]). *The nonlinear system* (10), *with the assumption* $\operatorname{rank}\{[b_1 \ \ldots \ b_m]\} = m$, *is feedback linearizable in an open and dense set* W_Y *of* $\mathbb{R}^n$ *if, and only if, the following conditions are satisfied*:

(1) *For each* $i = 0 \ldots n-1$, *the distribution* G_i *has constant dimension in* W_Y, *where* G_i *is defined as*

$$G_i = \operatorname{span}\left\{ad_A^k b_j,\ 0 \leqslant k \leqslant i,\ 1 \leqslant j \leqslant m\right\}, \tag{13}$$

where the Lie brackets of b_j *with respect to* A, *denoted by* $ad_A^k b_j$, *are defined as*

$$\begin{aligned} ad_A^k b_j &= \left[A, ad_A^{k-1} b_j\right] \\ &= \frac{\partial (ad_A^{k-1} b_j)}{\partial Y} A - \frac{\partial a}{\partial Y} ad_A^{k-1} b_j, \quad k \geqslant 1,\ ad_A^0 b_j = b_j, \end{aligned} \tag{14}$$

where $\partial A/\partial Y$ *and* $\partial b_j/\partial Y$ *denote the Jacobian of* $A(\cdot)$ *and* $b_j(\cdot)$, *respectively.*

(2) *The distribution* G_{n-1} *has dimension* n *in* W_Y.

(3) *For each* $i = 0, \ldots, n-2$, *the distribution* G_i *is involutive in* W_Y.

To transform the system (10) into the form of (12), we start by verifying the three conditions of Theorem 1. Computing the vectors $ad_A^k b_j,\ k = 1, \ldots, 3,\ j = 1, 2$, and their Lie brackets, it can be shown that the system (10) satisfies all three conditions of Theorem 1 in the set $W_Y = \mathbb{R}^8$.

Also, by using the Frobenius Theorem [21] it is shown, that the transformation T is given by

$$T = [T_1 \ \ldots \ T_8]^{\mathrm{T}} = \left[\lambda_1 \ \lambda_2 \ L_A^1\lambda_1 \ L_A^1\lambda_2 \ L_A^2\lambda_1 \ L_A^2\lambda_2 \ L_A^3\lambda_1 \ L_A^3\lambda_2\right]^{\mathrm{T}}, \tag{15}$$

where the scalar functions $\lambda_1(Y)$ and $\lambda_2(Y)$ satisfy the following set of partial differential equations:

$$\frac{\partial\lambda_l}{\partial y_m} = 0, \quad 1 \leqslant l \leqslant 2, \ 3 \leqslant m \leqslant 8, \tag{16}$$

$$d_3\frac{\partial\lambda l}{\partial y_1} - (d_3 + d_2\cos y_2)\frac{\partial\lambda l}{\partial y_2} \neq 0, \quad 1 \leqslant l \leqslant 2, \tag{17}$$

$$(d_3 + d_2\cos y_2)\frac{\partial\lambda_l}{\partial y_1} - (d_1 + 2d_2\cos y_2)\frac{\partial\lambda_l}{\partial y_2} \neq 0, \quad 1 \leqslant l \leqslant 2. \tag{18}$$

Choosing $\lambda_1(Y) = y_1$ and $\lambda_2(Y) = y_2$, it can be easily verified that Equations (16)–(18) hold, which yields the following linearizing state transformation:

$$T(Y) = \left[q_1 \ q_2 \ \dot{q}_1 \ \dot{q}_2 \ \ddot{q}_1 \ \ddot{q}_2 \ \dddot{q}_1 \ \dddot{q}_2\right]^{\mathrm{T}}. \tag{19}$$

Note that the transformation, given in (19), is not a unique solution of the set of Equations (16)–(18). However, the chosen solution has the advantage that the new state space coordinates consist of the joint angles, angular speeds, angular accelerations, and angular jerks, which are physical system parameters that can be measured or computed. Therefore, the output equation of the transformed system dynamics will be linear, which facilitates the control design phase.

The dynamics of the transformed system are computed by solving Equation (1) for the motor position vector, differentiating twice and substituting into Equation (2), which yields

$$M(q)\frac{\mathrm{d}^4q}{\mathrm{d}t^4} + h_p + h_f + N(q)J^{\mathrm{T}}\ddot{F} = \tau = u. \tag{20}$$

Here $M(q)$ is a new inertia matrix, h_p is a vector the elements of which are nonlinear functions of $q, \ \dot{q}, \ \ddot{q}, \ \dddot{q}$, h_f is a vector the elements of which are nonlinear functions of $q, \ \dot{q}, \ \ddot{q}, \ F, \ \dot{F}$, and $N(q)$ is a new matrix the elements of which are functions of the inertial parameters of the links and motors and joint stiffness. The system given by Equation (20) can be written in a state space form as

$$\dot{x} = f(x) + g(\bar{x}_1)\tau, \qquad x = \left[\bar{x}_1 \ \bar{x}_2 \ \bar{x}_3 \ \bar{x}_4\right]^{\mathrm{T}} = \left[q \ \dot{q} \ \ddot{q} \ \dddot{q}\right]^{\mathrm{T}}, \tag{21}$$

where $q = [q_1 \ q_2]^{\mathrm{T}}$. This model will be used in the control development presented in Section 5.

4. Constraint Frame and Forces for Decoupling

When dealing with rigid robots, it is sufficient to transform the link angular acceleration and the contact force into the constraint frame in order to obtain the decoupled systems. However, for flexible joints robot system, the fourth derivative of the link angular position vector and the second derivative of the contact forces must be transformed into the constraint frame in order to obtain the decoupled systems. In this section, the required transformations are derived. Note that in this paper, only planar constraint surfaces are considered.

Assume that there are m ($m \leqslant 2$) independent constraint frictionless surfaces which are holonomic and given by an algebraic equation, in the reference frame, in the form of

$$\phi_i(X) = 0, \quad i = 1, \ldots, m, \tag{22}$$

where Y is the end-effector position vector in the reference frame. Differentiating the constraint equation with respect to time yields the equation describing the end-effector velocity in the reference frame, yields

$$R_f \dot{X} = 0, \tag{23}$$

where the matrix R_f is defined as

$$R_f = [e_{6-m+1} \ \ldots \ e_6]^{\mathrm{T}}, \quad e_{6-m+i} = \frac{\mathrm{d}\phi_i(X)/\mathrm{d}X}{\|\mathrm{d}\phi_i(X)/\mathrm{d}X\|}. \tag{24}$$

Note that e_{6-m} is a unit vector normal to the constraint surface (22). Assuming that there exists a set of vectors $(e_1, \ldots, e_{6-m})$ such that e_i, $i = 1, \ldots, 6-m$, are of unit length, differentiable functions of X, mutually independent, and independent of $(e_{6-m+1}, \ldots, e_6)$, then the following two rotational matrices can be defined:

$$R_p = [e_1 \ \ldots \ e_{6-m}]^{\mathrm{T}}, \qquad R = \begin{bmatrix} R_p \\ R_f \end{bmatrix} = [e_1 \ \ldots \ e_6]^{\mathrm{T}}. \tag{25}$$

The matrix R_f represents the coordinate axes normal to the constraint surfaces, while the matrix R_p represents the coordinate axes that complement R_f. The coordinate system with its origin at the current end-effector position X and with the unit bases $(e_1, \ldots, e_{6-m})$ defines the constraint frame. Note that the matrices R_f and R_p are orthogonal. The rotation matrix R is the velocity transformation matrix from the reference frame into the constraint frame. This transformation and its derivatives are given by

$$\begin{aligned} &\dot{X}_t = R\dot{X}, \qquad \ddot{X}_t = R\ddot{X} + \dot{R}\dot{X}, \qquad \dddot{X}_t = \dddot{R} + 2\dot{R}\ddot{X} + \ddot{R}\dot{X}, \\ &\frac{\mathrm{d}^4 X_t}{\mathrm{d}t^4} = R\frac{\mathrm{d}^4 X}{\mathrm{d}t^4} + 3\big(\ddot{R}\ddot{X} + \dot{R}\dddot{X}\big) + \dddot{R}\dot{X}, \end{aligned} \tag{26}$$

where X_t is the end effector position in the constraint frame. The expression of the link position 4th derivative in the constraint frame is computed using the forward kinematic transformations, which yields

$$\frac{\mathrm{d}^4 q}{\mathrm{d}t^4} = J^{-1}\left[R^{-1}\left(\frac{\mathrm{d}^4 X_t}{\mathrm{d}t^4} - a_x\right) - a_q\right], \tag{27}$$

where a_q and a_x are given by

$$a_q = 3\big(\dot{J}\ddot{q} + \ddot{J}\dot{q}\big) + \dddot{J}\dot{q}, \qquad a_x = 3\big(\dot{R}\ddot{X} + \ddot{R}\dot{X}\big) + \dddot{R}\dot{X}. \tag{28}$$

It should be noted that

$$\frac{\mathrm{d}^4 X_t}{\mathrm{d}t^4} = \left[\frac{\mathrm{d}^4 P}{\mathrm{d}t^4} \quad 0\right]^{\mathrm{T}}, \tag{29}$$

where P is the end-effector position vector tangential to the constraint surfaces. This relationship states that the end-effector velocity and its higher order derivatives normal to the constraint surfaces are zero because the end-effector cannot penetrate the planar constraining surfaces considered in this paper.

The end-effector velocity $\dot{X}$ can be expressed in the reference frame as a 6-dimensional vector V consisting of a transnational and a rotational along each axis as follows:

$$V = T_v \dot{X}, \tag{30}$$

where T_v is a 6×6 transformation matrix. It can be shown that the transformation of the contact force and its derivatives, from the reference frame to the constraint frame, are given by

$$\begin{aligned} F &= (R_f T_v^{-1})^{\mathrm{T}} f_f \triangleq L f_f, \\ \dot{F} &= L\dot{f}_f + L f_f, \\ \ddot{F} &= L\ddot{f}_f + 2\dot{L}\dot{f}_f + \ddot{L} f_f \triangle L\ddot{f}_f + a_f, \end{aligned} \tag{31}$$

where f_f represents the contact force vector F in terms of the unit vector L which is normal to the constraint surfaces. Equation (26) gives the expression of the contact force vector F due to the vector force f_f, at the tip of the end-effector, in the reference frame. The contact force f_f is normal to the constraint surfaces and it is the negative equivalent of the Lagrangian multiplier κ, i.e., $f_f = -\kappa$. It should be noted that Equation (26) does not prescribe the manner in which the force vector and its first two derivatives are obtained, but enables the transformation of these vectors from the constraint frame into the reference frame. The contact force f_f can be computed using the constraint and the rigid dynamics of the robot, which yields

$$f_f = \big(R_f J D^{-1} J^{\mathrm{T}} L\big|^{-1}\big[R_f J D^{-1} h_1 + R_f \dot{J}\dot{q} + \dot{R}_f J\dot{q}\big]\big), \tag{32}$$

where the function $h_1(\cdot)$ yields from the substitution of (31) into (20) and using (1) and (2).

5. Robust Sliding Mode Controller Design

5.1. BASIC CONCEPT

Sliding mode control methodology has emerged as a promising technique for designing robust controllers for a class of nonlinear systems. This technique is based on choosing a suitable surface in the state space, typically a linear hypersurface called switching surface, and switching the control input on this surface. The control input is then chosen such that the trajectories near the sliding surface are guaranteed to be directed towards the surface. Once the system is trapped on the surface, the closed loop dynamics are completely governed by the equations that define the surface. Therefore, since the parameters defining the surface are chosen by the designer, the closed-loop dynamics of the system will be independent of the perturbations in the system parameters and robustness will be achieved [24]. The design of the sliding mode controller consists of three steps. First, sliding surfaces are defined for the position and force subsystems. Then, a nominal control law is designed for the nominal model, without including the effect of system parameter variations. Finally, the nominal control law is modified by adding a switching term based on the sign of the error in the position and force subsystems and bounds of the disturbance vector.

5.2. CONTROLLER DESIGN

As mentioned previously, the sliding surfaces have to be defined. Let s_{pi} and s_{fi} be the sliding surfaces for the position and force tracking errors, respectively, expressed in the constraint frame as

$$s_{pi} = \left(\frac{\mathrm{d}}{\mathrm{d}t} + \kappa_{pi}\right)^2 \int_0^t z_{pi}\,\mathrm{d}r, \quad i = 1, \ldots, 6-m, \tag{33}$$

$$s_{fi} = \left(\frac{\mathrm{d}}{\mathrm{d}t} + \kappa_{fi}\right)^2 \int_0^t z_{fi}\,\mathrm{d}r, \quad i = 1, \ldots, 6-m+1, \ldots, 6, \tag{34}$$

where z_{pi} and z_{fi} are the ith end-effector position and force tracking errors in the constraint frame and κ_{pi} and κ_{fi} are positive scalar constants. The appropriate control law, with which the desired performance is achieved, has to satisfy the following sliding condition:

$$\dot{s}_{pi} = 0, \quad i = 1, \ldots, 6-m, \tag{35}$$

$$\dot{s}_{fi} = 0, \quad i = 6-m+1, \ldots, 6. \tag{36}$$

Conditions (35) and (36) guarantee that the position and force tracking errors converge to zero. Expanding Equations (35), (36), using Equations (33) and (34), we

have that

$$\dot{s}_{pi} = \frac{\mathrm{d}^4 z_{pi}}{\mathrm{d}t^4} + 4\kappa_{pi}\frac{\mathrm{d}^3 z_{pi}}{\mathrm{d}t^3} + 6\kappa_{pi}^2\frac{\mathrm{d}^2 z_{pi}}{\mathrm{d}t^2} + + 4\kappa_{pi}^3\frac{\mathrm{d}z_{pi}}{\mathrm{d}t} + \kappa_{pi}^4 z_{pi} = 0, \qquad i = 1, \ldots, 6-m, \tag{37}$$

$$\dot{s}_{fi} = \frac{\mathrm{d}^2 z_{fi}}{\mathrm{d}t^2} + 2\kappa_{fi}\frac{\mathrm{d}z_{fi}}{\mathrm{d}t} + \kappa_{fi}^2 z_{fl} = 0, \quad i = 6-m+1, \ldots, 6. \tag{38}$$

Define the vectors S_p, S_f, and S as follows:

$$S_p = [s_{p1} \ \ldots \ s_{p6-m}]^{\mathrm{T}}, \qquad S_f = [s_{f6-m+1} \ \ldots \ s_{f6}]^{\mathrm{T}}, \quad S = [S_p^{\mathrm{T}} \ S_f^{\mathrm{T}}]^{\mathrm{T}}. \tag{39}$$

The nonlinear robot model (20)–(21) can be rewritten to augment the position and force in the constraint frame as

$$\begin{aligned}\tau &= u \\ &= H(q)\begin{bmatrix}\dfrac{\mathrm{d}^4 P}{\mathrm{d}t^4} \\ \dfrac{\mathrm{d}^2 f}{\mathrm{d}t^2}\end{bmatrix} + h_p(q, \dot{q}, \ddot{q}, q) + h_f\big(q, \dot{q}, \ddot{q}, F, \dot{F}\big) + \\ &\quad + MJ^{-1}\big(R^{-1}a_x - a_q\big) + NJ^{\mathrm{T}}a_f,\end{aligned} \tag{40}$$

where P is $(6-m)\times 1$ end-effector position vector tangential to the constraint surface, R is the velocity transformation from the reference frame into the constraint frame, defined in the Section 4, $H(q)$ is a matrix whose first $(6-m)$ columns are the first $(6-m)$ columns of the matrix $M(RJ)^{-1}$ and the remaining columns are those of the matrix $NJ^{\mathrm{T}}L$. By solving the sliding conditions (37) and (38) for the fourth position derivative and the second force derivative and substituting into (40) we get the control law:

$$\begin{aligned}\tau &= u \\ &= H(q)\begin{bmatrix}\dfrac{\mathrm{d}^4 P_d}{\mathrm{d}t^4} + 4\kappa_p\dfrac{\mathrm{d}^3 z_p}{\mathrm{d}t^3} + 6\kappa_p^2\dfrac{\mathrm{d}^2 z_p}{\mathrm{d}t^2} + 4\kappa_p^3\dfrac{\mathrm{d}z_p}{\mathrm{d}t} + \kappa_p^4 z_p \\ \ddot{f}_d + 2\kappa_f\dot{z}_f + \kappa_f^2 z_f\end{bmatrix} + \\ &\quad + h_p(\cdot) + h_f(\cdot) + MJ^{-1}\big(R^{-1}a_x - a_q\big) + NJ^{\mathrm{T}}a_f \\ &\quad \triangleq H(q)\Gamma(\cdot) + h_p(\cdot) + h_f(\cdot) + MJ^{-1}\big(R^{-1}a_x - a_q\big) + NJ^{\mathrm{T}}a_f,\end{aligned} \tag{41}$$

where P_d and f_d are the desired end-effector position vector tangential to the constrained frame and the desired contact forces, respectively. The control law (41) satisfies the sliding conditions (37) and (38), when the system parameters are exactly known and, hence, the desired system performance can be achieved. However, in the presence of parameter uncertainties, the control law (41) can no longer guarantee the achievement of the desired position nor the force tracking performance. In such case, the control torque can best be computed using an estimate or

approximation of the robot parameters, i.e., Equation (41) is modified as:

$$\begin{aligned}\hat{\tau} &= \widehat{H}(q)\begin{bmatrix} \dfrac{\mathrm{d}^4 P_d}{\mathrm{d}t^4} + 4\kappa_p \dfrac{\mathrm{d}^3 \hat{z}_p}{\mathrm{d}t^3} + 6\kappa_p^2 \dfrac{\mathrm{d}^2 \hat{z}_p}{\mathrm{d}t^2} + 4\kappa_p^3 \dfrac{\mathrm{d}\hat{z}_p}{\mathrm{d}t} + \kappa_p^4 \hat{z}_p \\ \ddot{f}_d + 2\kappa_f \dot{z}_f + \kappa_f^2 z_f \end{bmatrix} + \\ &\quad + \hat{h}_p(\cdot) + \hat{h}_f(\cdot) + \widehat{M} J^{-1}\big(R^{-1}\hat{a}_x - a_q\big) + \widehat{N} J^{\mathrm{T}} \hat{a}_f \\ &\triangleq \widehat{H}(q)\widehat{\Gamma}(\cdot) + \hat{h}_p(\cdot) + \hat{h}_f(\cdot) + \widehat{M} J^{-1}\big(R^{-1}\hat{a}_x - a_q\big) + \widehat{N} J^{\mathrm{T}} \hat{a}_f. \end{aligned} \tag{42}$$

The control law (42) is similar to the dynamic hybrid control law except that the former uses the estimated robot parameters. In order to satisfy the sliding conditions (35), (36), despite the presence of uncertainties in the robot parameters, the control law (41) is modified by adding a discontinuous term across each of the surfaces $S_p = 0$ and $S_f = 0$. Thus, the robust control law is given by:

$$\tau = u = \hat{\tau} - \widehat{H}(q) K_d \operatorname{sgn}(S), \tag{43}$$

where $\hat{\tau}$ is given in (42), S is defined in (54), K_d is the switching gain matrix which is a positive definite diagonal matrix, and $\operatorname{sgn}(S)$ is a vector defined as:

$$\begin{aligned}\operatorname{sgn}(S) &= [\operatorname{sgn}(S_p)\ \operatorname{sgn}(S_f)]^{\mathrm{T}} \\ &= \big[\operatorname{sgn}(s_{p1})\ \ldots\ \operatorname{sgn}(s_{p6-m})\ \operatorname{sgn}(s_{f6-m+1})\ \ldots\ \operatorname{sgn}(s_{f6})\big]^{\mathrm{T}}, \end{aligned} \tag{44}$$

where sgn is the sign function defined by:

$$\operatorname{sgn}(x) = \begin{cases} +1 & \text{if } x > 0, \\ -1 & \text{if } x < 0. \end{cases} \tag{45}$$

The design of the switching gain matrix K_d which ensures the availability of the sign vector in (43) is presented next. The control law (43) can be rearranged in a way that enables computing an upper bound for the disturbance as follows:

$$\begin{aligned}\tau &= \widehat{H}(q)\Gamma(\cdot) + \hat{g}\big(q, \dot{q}, \ddot{q}, \dddot{q}, F, \dot{F}\big) + \widehat{H}(q)\delta\big(\dddot{z}_p, \ddot{z}_p, \dot{z}_f, \dddot{\hat{z}}_p, \ddot{\hat{z}}_p, \dot{\hat{z}}_f\big) - \\ &\quad - \widehat{H}(q) K_d \operatorname{sgn}(S), \end{aligned} \tag{46}$$

where $\Gamma(\cdot)$ is defined in (45), $\dot{z}_f$, $\ddot{z}_p$, $\dddot{z}_p$ are the estimate of $\dot{z}_f$, $\ddot{z}_p$, $\dddot{z}_p$ which will be discussed in the following section, and the vector functions $\hat{g}(\cdot)$ and $\delta(\cdot)$ are given by:

$$\begin{aligned}\hat{g}\big(q, \dot{q}, \dddot{q}, F, \dot{F}\big) &= \hat{h}_p\big(q, \dot{q}, \ddot{q}, \dddot{q}\big) + \hat{h}_f\big(q, \dot{q}, \ddot{q}, F, \dot{F}\big) + \\ &\quad + \widehat{M} J^{-1}\big[R^{-1}\hat{a}_x - q_q\big] + \widehat{N} J^{\mathrm{T}} \hat{a}_f, \end{aligned} \tag{47}$$

$$\delta\big(\dddot{z}_p, \ddot{z}_p, \dddot{\hat{z}}_p, \ddot{\hat{z}}_p, \dot{z}_f, \dot{\hat{z}}_f\big) = \begin{bmatrix} 4\kappa_p(\dddot{z}_p - \dddot{\hat{z}}_p) + 6\kappa_p^2(\ddot{z}_p - \ddot{\hat{z}}_p) \\ 2\kappa_f(\dot{z}_f - \dot{\hat{z}}_f) \end{bmatrix}. \tag{48}$$

Define the matrices $\widetilde{H} = H - \widehat{H}$ and $\Delta = H^{-1}\widetilde{H}$. Then the matrix $\widehat{H}$ can be expressed as $\widehat{H} = H(\Delta + I)$. The sliding conditions (35), (36) are modified from plane surfaces to hyperplanes with some thickness as:

$$|S| \leqslant \mu, \qquad \mu \triangle [\mu_p\ \mu_f]^{\mathrm{T}} \triangle [\mu_{p1}\ \ldots\ \mu_{pm-6}\ \mu_{f6-m+1}\ \ldots\ \mu_{f6}]^{\mathrm{T}}, \tag{49}$$

where the μ_i's are strictly positive constants. When the control law (46) is applied, the following error dynamics results:

$$H(q)\dot{S} = H(q)\pi(t) - H(D+I)K_d\text{sgn}(S), \tag{50}$$

where the function $\pi(t)$ is a disturbance term given by

$$\pi(t) = -\left(H^{-1}\tilde{g}\left(q, \dot{q}, \ddot{q}, \dddot{q}, F, \dot{F}\right) + (D+I)\delta\left(\dddot{z}_p, \ddot{z}_p, \dddot{\hat{z}}_p, \ddot{\hat{z}}_p\right) + D\Gamma(\cdot)\right) \tag{51}$$

and the function $\widehat{\Gamma}(\cdot)$ is defined in (42). It can be seen that if the gain matrix K_d satisfies the condition

$$(D+I)K_d \geqslant \mu + \pi(t), \tag{52}$$

then the sliding conditions, given by (49), are satisfied, which yields

$$\frac{1}{2}\frac{\mathrm{d}}{\mathrm{d}t}S^2 \leqslant -\mu|S|. \tag{53}$$

Condition (53) states that the squared distance, measured by S^2, decreases along the trajectories. Thus, this condition constrains the trajectories to point toward the surface S.

In order to determine the upper bound of the disturbance $\pi(t)$ and investigate the knowledge of the sign of the sliding surfaces, the estimate of x, where x is defined in (21), must be computed first.

5.3. ESTIMATION OF THE TRANSFORMED STATE VECTOR x

In this section, a simple solution to the problem of estimating the transformed state vector x is presented. First, rewrite the system (20)–(21), in the x-state space coordinate, as:

$$\dot{x} = \begin{bmatrix} 0 & I_{2\times2} & 0 & 0 \\ 0 & 0 & I_{2\times2} & 0 \\ 0 & 0 & 0 & I_{2\times2} \\ 0 & 0 & 0 & 0 \end{bmatrix} x + \begin{bmatrix} 0 \\ 0 \\ 0 \\ I_{2\times2} \end{bmatrix} v \triangleq A_L x + B_L v, \tag{54}$$

where the expression of the control input v satisfies

$$v = M^{-1}(q)\tau - M^{-1}(q)\left[h_p(\cdot) + h_f(\cdot) + N(q)J^{\mathrm{T}}\ddot{F}\right] \triangleq \alpha(x)u + \beta(x). \tag{55}$$

The new state vector x consists of the joint angles q, angular velocities $\dot{q}$, angular accelerations $\ddot{q}$, and angular jerks $\dddot{q}$. In general, sensors that provide measurements of the joint angles and angular speeds are commonly available in most robot manipulator systems. However, sensors which provide accurate measurements of the accelerations are not usually utilized due to their high cost. In addition, the jerks can not be measured or computed with high accuracy. In order to reduce

the cost of the proposed nonlinear controller, compared with the cost of existing ones, it is assumed that only measurements of the joint angles and angular speeds are available. Therefore, the outputs of the original system and the linear transformed system are given by

$$Y_L = \begin{bmatrix} I_{2\times2} & 0_{2\times2} & 0_{2\times2} & 0_{2\times2} \\ 0_{2\times2} & I_{2\times2} & 0_{2\times2} & 0_{2\times2} \end{bmatrix} x + \eta_s \triangle C_L Y + \eta_s, \tag{56}$$

where η_s represents the measurement noise which is assumed to be a Gaussian process with zero mean and covariance R_s.

Existing solutions for estimating the transformed state vector use measurements of the full original nonlinear state vector Y along with the analytical expression of linearizing transformation. This approach is effective when the measurements are noise free. However, in the presence of measurement noise, which is often the case, such a solution may lead to inaccurate estimates. One way to modify this solution, in the case of noisy measurements, is to determine the conditional probability density function of Y given the measurement vector Y_L, $P_y(Y/Y^L)$. Then, the conditional probability density function of the transformed state can be computed using the analytical expression of the linearizing transformation along with $P_y(Y/Y_L)$. This approach requires solving Kushner Equation [25] for $P_y(Y/Y_L)$. In general, an analytical solution is very difficult to find for such equation. However, the problem of computing the estimate of x can be solved in a simpler way by taking advantage of the linear form of the transformed system dynamics (54)–(56). Given the measurements vector Y_L and the control input v, computed using (55), a linear optimal observer (Kalman filter) can be designed to generate an estimate of the transformed state x, $\hat{x}$, using linear quadratic estimation techniques (LQE). The estimate $\hat{x}$ becomes the output of the state estimator whose dynamics are given by

$$\frac{\mathrm{d}}{\mathrm{d}t}\hat{x} = (A_L - K_f C_L)\hat{x} + B_L v + K_f Y_L, \tag{57}$$

where A_L, B_L, C_L, v, and Y_L are defined in (54)–(56) and K_f, is the estimator gain given by

$$K_f = P_f C_L^{\mathrm{T}} R_f^{-1}, \quad R_f > 0. \tag{58}$$

The matrix P_f is the unique solution of the Ricatti equation

$$P_f A_L^{\mathrm{T}} + A_L P_f - P_f C_L^{\mathrm{T}} R_f^{-1} C_L P_f = 0, \tag{59}$$

where Q_f and R_f are the observer design parameters. The choice of the weighing matrices Q_f and R_f is based on the following criteria: (a) good tracking performance, and (b) the cross-over frequency of the LQE return ratio $L(s)$, defined as $L(s) = -C[sI - A]^{-1}K_f$, is less than the frequency bandwidth of the system, w_b. These constraints are necessary for noise rejection and to guarantee robustness

towards unmodeled dynamics and model uncertainties, which become active for frequencies above w_b [22].

Given that the error in estimating the state vector x is guaranteed to be bounded, using the LQE design, then the end-effector position error in the constraint frame is also guaranteed to be bounded; that is there exist positive constants σ_1 and σ_2 such that

$$\left\|\ddot{z}_p - \hat{\ddot{z}}_p\right\| \leqslant \sigma_1, \qquad \left\|\dddot{z}_p - \hat{\dddot{z}}_p\right\| \leqslant \sigma_2. \tag{60}$$

These relationships state that the difference between the true and estimated state vector is bounded.

Since the force and its first derivative, Equation (46), are continuous functions of the state x and the robot parameter vector Θ, an upper bound for the force first derivative can be derived as

$$\left\|\dot{f}_f - \hat{\dot{f}}_f\right\| = \left\|T_f(Y, \Theta) - T_f\left(Y, \widehat{\Theta}\right)\right\| \leqslant J_{Tf}(Y)\left\|\widehat{\Theta}\right\|, \tag{61}$$

where the transformation $T_f(\cdot)$ is defined as

$$T_f(Y, \Theta) = \dot{f}_f, \qquad J_{Tf} = \text{Jacobian}(T_f), \tag{62}$$

where J_{Tf} is evaluated with respect to Θ. Since the error in the state estimate and the force derivative are bounded, an upper bound of the disturbance vector $\pi(t)$ exists. This enables the design of the switching gain K_d which satisfies (52). Next, the properties of the sliding surfaces are studied.

5.4. THE SLIDING SURFACE PROPERTIES

In this section, the bounds of the estimation error are combined with the properties of the sliding surface in order to obtain a range in which the sliding mode control can be applied. This requires the introduction of the boundary layer concept. In practical applications, discontinuous control laws are known to generate very high control activity which should be avoided. As a result, the objective of the surface being converging to zero is replaced by keeping the surface within certain limits that define the boundary layer thickness. The thickness of the boundary layer is determined by the tracking errors. Outside the boundary layer, the control input is applied while inside the boundary layer the control is interpolated as:

$$\tau = \hat{\tau} - K_d \,\text{sat}(S/\phi_s), \tag{63}$$

where ϕ_s is a scalar positive constant that defines the boundary layer thickness and sat is the saturation function defined as

$$\text{sat}(x) = \begin{cases} x & \text{if } x \leqslant 1, \\ \text{sgn}(x) & \text{if } x > 1. \end{cases} \tag{64}$$

Thus, instead of aiming at $S = 0$ one aims at having

$$\|S\| \leqslant \phi_s. \tag{65}$$

Note that the choice of ϕ_s depends on the availability of the transformed state vector as well as the uncertainties in the system parameters. The relationship between the minimum boundary layer thickness and the maximum error in S, due to parameter uncertainties, can be derived. The true sliding surfaces for the position and force tracking errors, defined in (35) and (36), can be decomposed into an estimated part and a measured part as follows:

$$S = S_u + S_n, \qquad \widehat{S} = \widehat{S}_u + \widehat{S}_n, \tag{66}$$

where

$$\begin{aligned} S_u &= \begin{bmatrix} \dddot{z}_p + 4\kappa_p \ddot{z}_p \\ \dot{z}_f \end{bmatrix}, \qquad \widehat{S}_u = \begin{bmatrix} \dddot{z}_p + 4\kappa_p \ddot{z}_p \\ \dot{z}_f \end{bmatrix}, \\ S_n &= \begin{bmatrix} 6\kappa_p^2 \dot{z}_p + 4\kappa_p^3 z_p + \kappa_p^4 \int_0^t z_p \\ 2\kappa_f \dot{z}_f + \kappa_f^2 \int_0^t z_f \end{bmatrix}. \end{aligned} \tag{67}$$

Computing the term $S - \widehat{S}$, yields

$$S - \widehat{S} = \delta_s(t) \triangleq \begin{bmatrix} (\dddot{z}_p - \dddot{\hat{z}}_p) + 4\kappa_p(\ddot{z}_p - \ddot{\hat{z}}_p) \\ \dot{z}_f - \dot{z}_f \end{bmatrix}. \tag{68}$$

Using the fact that the error in estimating the state vector x is guaranteed to be bounded and the properties of the force derivative expression given in (61), yields the following upper bound for the error in S:

$$\| S - \widehat{S} \| = \| S_u - \widehat{S}_u \| = \| \delta_s(t) \| \leqslant \sigma_s, \quad \text{where } \sigma_s \geqslant \left\| \begin{matrix} \sigma_2 + 4\kappa_p \sigma_1 \\ \sigma_f \end{matrix} \right\|, \tag{69}$$

where σ_f is defined as

$$\| \dot{z}_f - \dot{z}_f \| \leqslant \sigma_f. \tag{70}$$

It is clear, by inspecting the bounds on the sliding surfaces, that the boundary layer ϕ_s cannot be smaller than σ_s. Thus, the boundary layer thickness satisfies:

$$S \leqslant \phi_s \leqslant 2\sigma_s. \tag{71}$$

Note that it is possible to force the true surface S to remain inside the above boundary layer since $\widehat{S}$ is known. Equation (68) can be written as:

$$S = \widehat{S}_u + \sigma_s(t). \tag{72}$$

Outside the boundary layer we have:

$$\widehat{S} > \sigma_s \Rightarrow \operatorname{sgn}(S) = \operatorname{sgn}\big(\widehat{S}\big). \tag{73}$$

Thus, the discontinuous control input can force the system to satisfy the sliding conditions inside the boundary layer where

$$S < 2\sigma_s, \qquad \widehat{S} < \sigma_s, \qquad S \approx \widehat{S}. \tag{74}$$

6. Experimental Tests

6.1. THE EXPERIMENTAL SETUP

The experimental setup used to implement the above controllers consists of a mechanical arm and a real time controller. The mechanical arm, illustrated in Figure 1, is a two link modular direct drive manipulator which has been designed and built to truly simulate the effects of the joint flexibility. Helical torsional springs are used in the joint's flexibility design. The current configuration has two resonant frequencies of 5.2 and 7.5 Hz. The robot is equipped with four encoders to read the positions of the motors and the links, and a force/torque sensor at the end effector. The real time controller was designed and built. It consists of a digital signal processing card based on the TMS320C30 chip which is interfaced through a bus to a number of input output devices for communication with robot sensors and motors. Details of the experimental robot can be found in [26]. Table 1 shows two lists of the robot parameters are obtained using I-DEAS solid modeler and sine sweep identification. Figure 2 shows the experimental flexible joints robot constrained by a rigid straight wall. The robot end-effector is equipped with a roller to satisfy the assumption that the wall is friction-free. The wall is made of a steel plate rigidly fixed to the robot table by two L-shaped supports. The controller was implemented and applied to the experimental flexible joint robot with a sampling frequency of 1 KHz. Parametric uncertainties were introduced by adding a 0.98 Kg steel block at the center of mass of the second link. Two experiments were performed.

6.2. EXPERIMENT 1: NOISE-FREE MEASUREMENTS

In this test, the measured variables are the links and the motors angular positions and velocities and the contact force. All measurements are assumed to be noise free. The links angular accelerations and jerks are computed using the analytical expression of the inverse transformation T^{-1}, where the expression of T is given

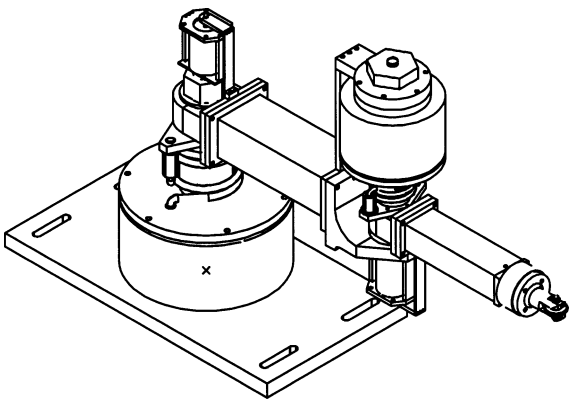

Figure 1. Solid model of the experimental flexible joints robot.

Table I. Experimental robot parameters

Robot parameters	I-DEAS	Sine sweep
l_1(m)	0.400	
l_2(m)	0.350	
d_1(Kg m^2)	2.110	2.087
d_2(Kg m^2)	0.223	0.216
d_3(Kg m^2)	0.085	0.084
b_1(N m s/rad)		2.041
b_2(N m s/rad)		0.242
b_{m1}(N m s/rad)		1.254
b_{m2}(N m s/rad)		0.119
k_1(N m/rad)	198.49	125.56
k_2(N m/rad)	51.11	31.27
I_{m1}(Kg m^2)	0.1226	0.1224
I_{m2}(Kg m^2)	0.017	0.0168

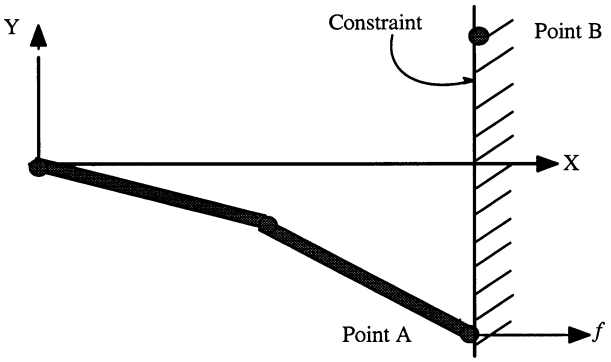

Figure 2. Layout of the experimental flexible joint robot constrained by a straight wall.

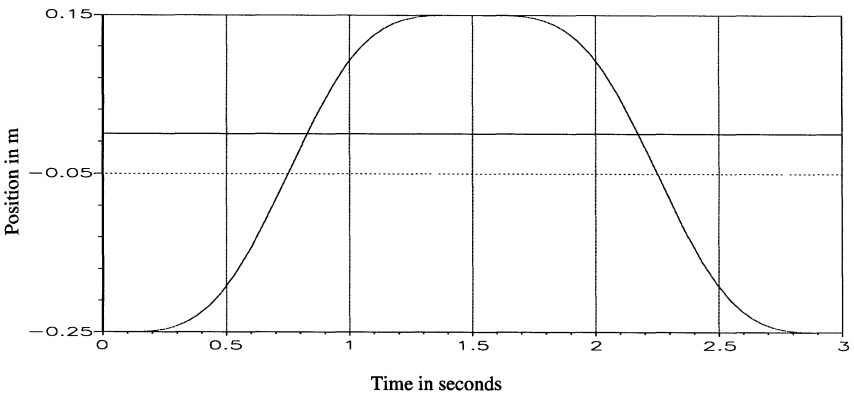

Figure 3. Desired position trajectory for the dynamic hybrid controller.

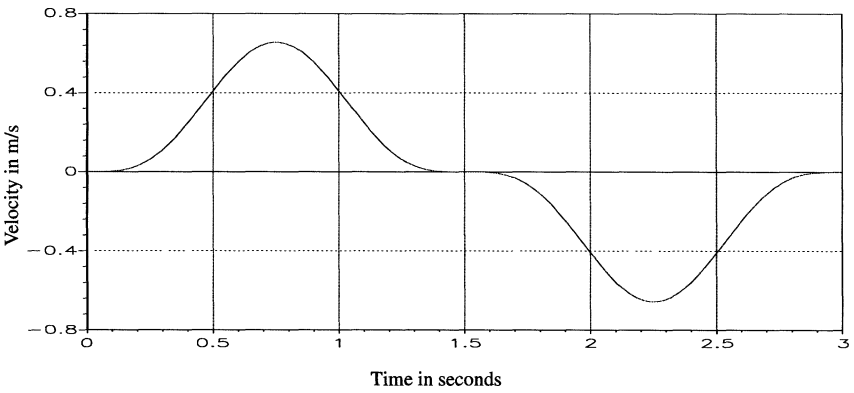

Figure 4. Desired velocity trajectory for the dynamic hybrid controller.

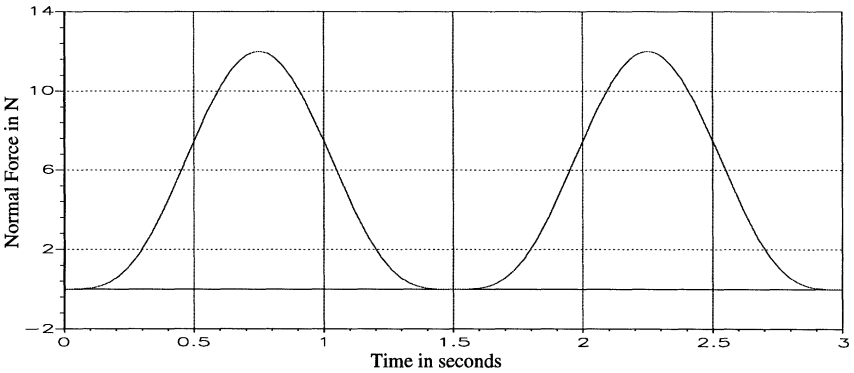

Figure 5. Desired force trajectory for the dynamic hybrid controller.

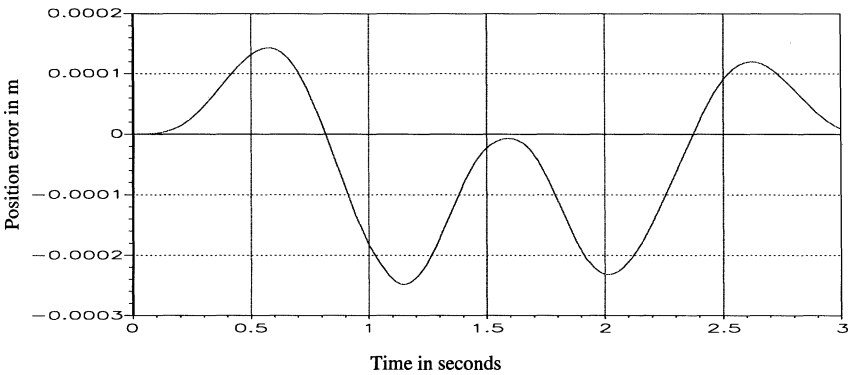

Figure 6. Position tracking error for the robust sliding mode controller (simulation).

in (19). The experiment layout is shown in Figure 2 and the task consists of moving the end-effector by 0.4 m (starting from point A to point B) in the Y-direction according to a smooth desired position trajectory while applying a desired force normal to the wall in 1.5 seconds, then to return to the initial point in another 1.5 seconds. The amplitude of the force is 12.0 N. The position and force surfaces

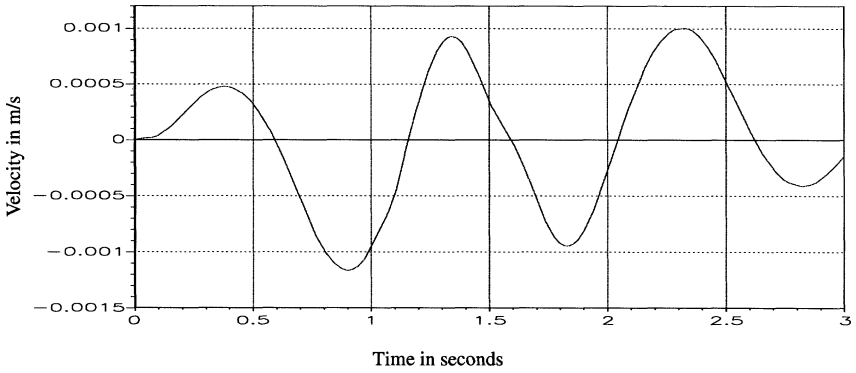

Figure 7. Velocity tracking error for the robust sliding mode controller (simulation).

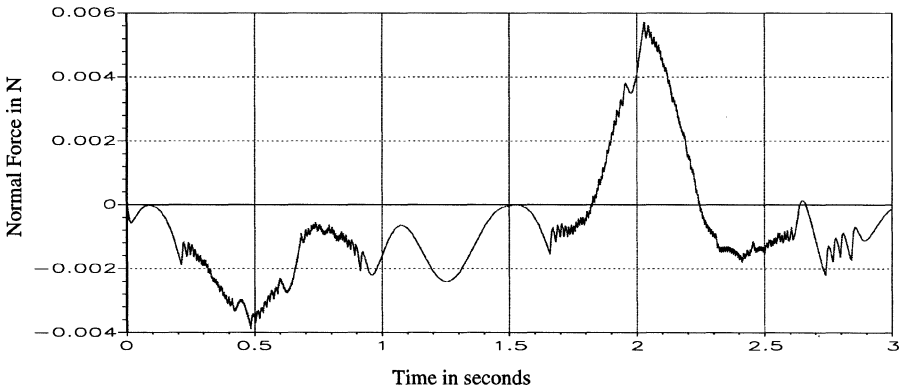

Figure 8. Force tracking error for the robust sliding mode controller (simulation).

are defined by $\kappa_p = 25$ and $\kappa_f = 60$. The boundary layer thickness is defined by $\phi_p \leqslant 2.0$ and $\phi_f \leqslant 5.0$. These values were computed using experimental tracking trajectories. Figures 3–5 shows the desired position, velocity, and force tracking trajectories. Figures 6–8 show the simulation results of the position, velocity, and force tracking errors. These figures indicate that the maximum errors are: 0.25 mm for the position, 1.25 mm/s for the velocity, and 0.006 N for the force. This demonstrates the good tracking performance provided by the proposed controller. Figures 9 and 10 show the experimental angular position and velocity tracking errors while Figure 11 shows the force tracking error. These figures indicate that the proposed controller managed to achieve satisfactory position, velocity, and force tracking (errors: less than 4 mm for the position and less than 0.04 m/s for the velocity) despite the presence of parameter uncertainties. The uncertainties were introduced by adding a 0.98 kg steel block at the center of mass of the second link. Note that there is some discrepancy between the experimental and simulation results. This is due to the fact that the effects of measurements noise are not taken into account in this first experiment.

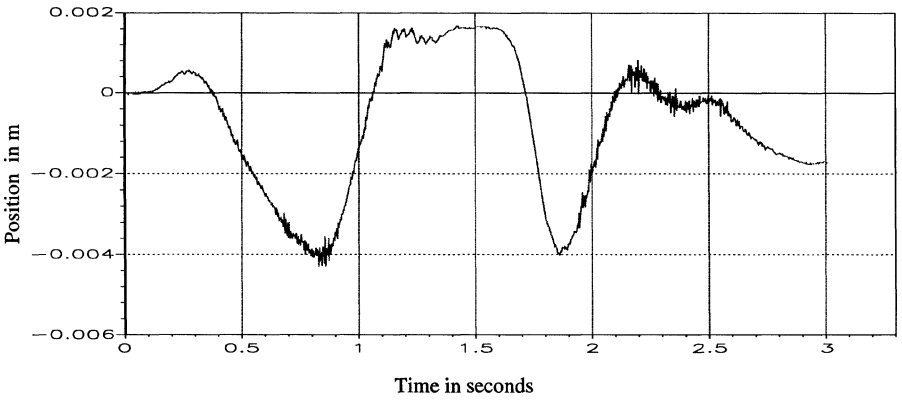

Figure 9. Position tracking error for the robust sliding mode controller (experimental).

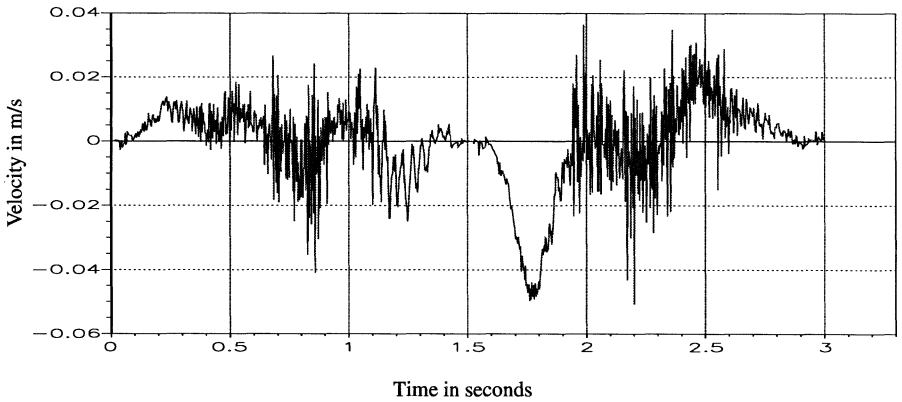

Figure 10. Velocity tracking error for the robust sliding mode controller (experimental).

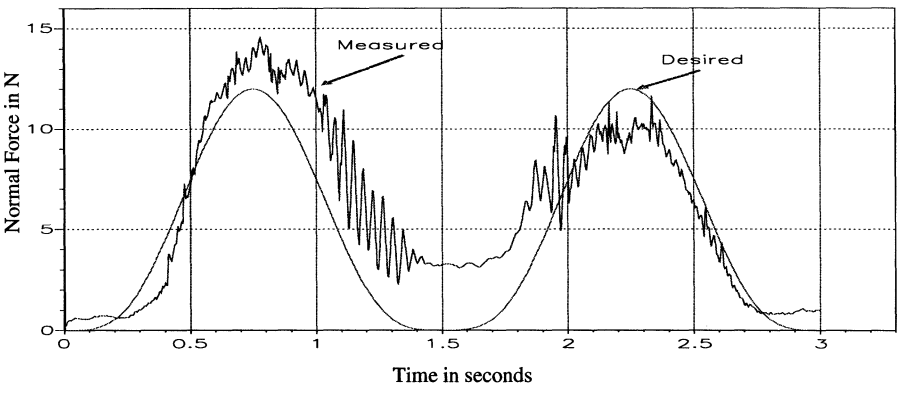

Figure 11. Force trajectory tracking for the robust sliding mode controller (experimental).

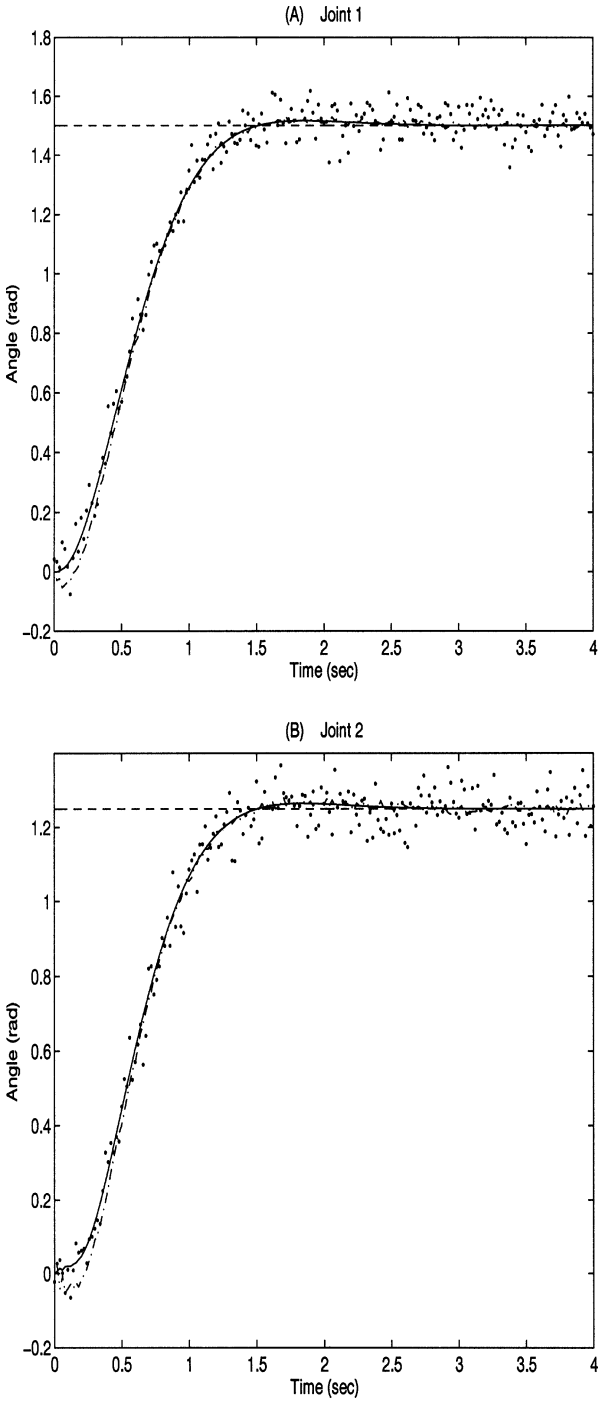

Figure 12. Joint's angular positions: - - - desired, — actual, -.-. estimate, · · · measured.

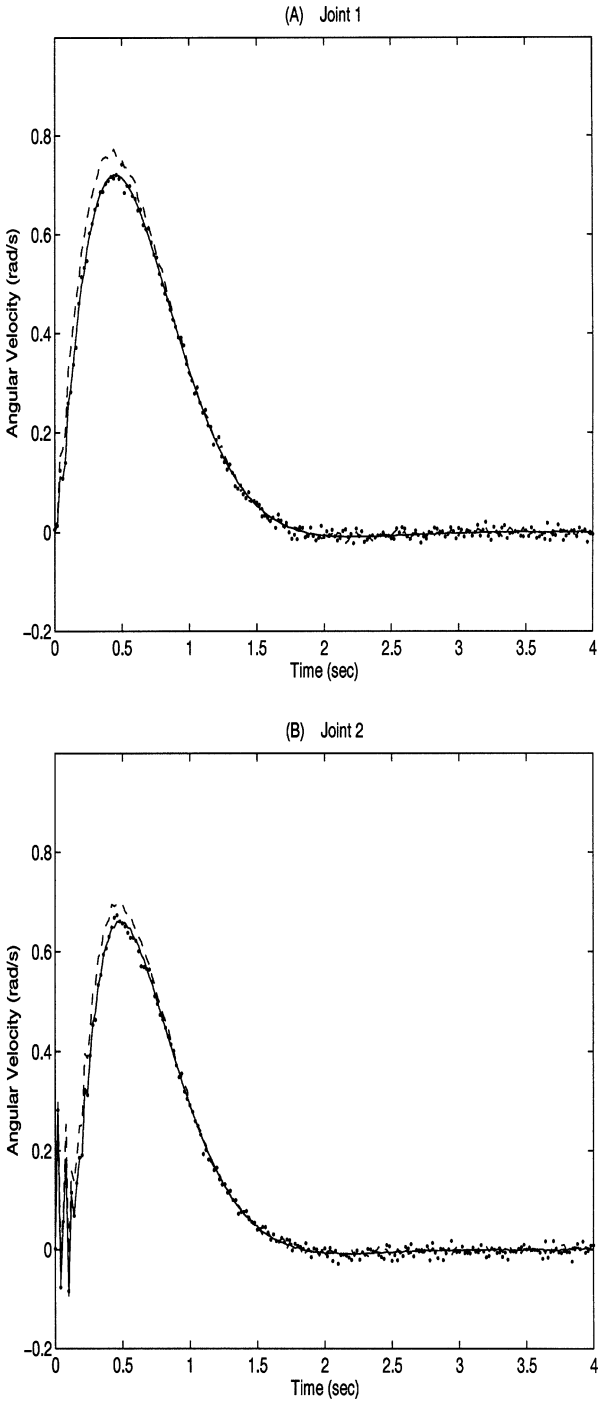

Figure 13. Joint's angular velocities: — actual, - - - estimate, · · · measured.

6.3. EXPERIMENT 2: NOISY MEASUREMENTS

In this second test, the controller was designed taking into consideration the measurement noise and assuming that only measurements of the links angular positions and velocities are available. A Gaussian noise is introduced in the measurements: $N \sim (0, 0.05)$ for the angular position and $N \sim (0, 0.01)$ for the angular velocity. The simulations results are shown in Figures 12–16. Figures 12 and 13 show plots of the measured, estimated, and actual angular positions and velocities of the two joints. These figures indicate that the system reaches the desired trajectory within 1.5 s without any overshoot, despite the presence of measurements noise. Figures 14 and 15 show plots of the actual and the estimated motor angular positions and velocities. These figures demonstrate that the state estimator derived in Section 5.3 is very simple, efficient and practical to use, since the estimated states converge within less than one second and with minimum of oscillations. Thus, with the proposed control approach, the use of sensors that measure the motor dynamics can be omitted without affecting the performance of the FL-based controller. Figure 16 shows that the desired performance can be achieved with reasonable control effort (the maximum control torque is less 5.0 NM for the first link and less 1.0 NM for the second link which are very reasonable for such tasks). These results clearly indicate that the proposed control approach is of potential benefits for the hybrid position and force control of flexible joints robot manipulator systems. Additional physical experiments are underway.

7. Conclusion

In this paper, a robust sliding mode controller was designed to control the position and force of flexible joints robot manipulators constrained by a rigid environment, in the presence of parameters uncertainty. The control law is derived using the concept of feedback linearization and sliding mode technique. The set over which the nonlinear flexible joint robot manipulator model (10) is feedback linearizable, was determined. The controller is composed of a switching and an equivalent control actions. The equivalent control action can achieve, in principle, perfect decoupling when the robot parameters are known. The switching control action was designed to compensate the closed loop error caused by the parametric uncertainty. It utilizes the bounds on the robot parameters to obtain an upper bound for the closed loop error which forces the position and force subsystems to remain on their sliding surfaces. The effect of estimating the unmeasured elements of the state vector of the feedback linearizable system (acceleration and jerk) and the contact forces first derivatives results in the existence of a limit for the minimum achievable boundary layer thickness, which is a direct measure of the tracking performance. The relation between the parametric uncertainty measure and the minimum achievable boundary layer thickness was obtained. Preliminary results show that the new approach for computing the state estimate, presented in Section 5.3, is very efficient in reducing the cost and the complexity of the controller design. Simulation and

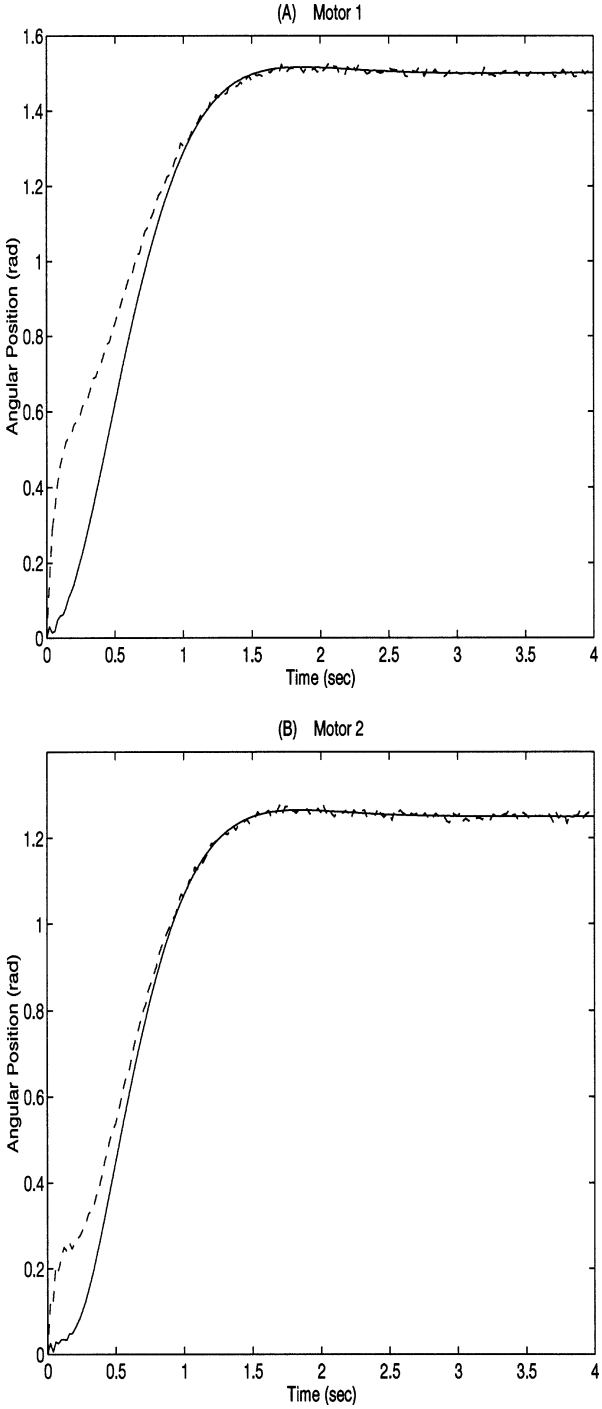

Figure 14. Motor's angular positions: — actual, - - - estimate.

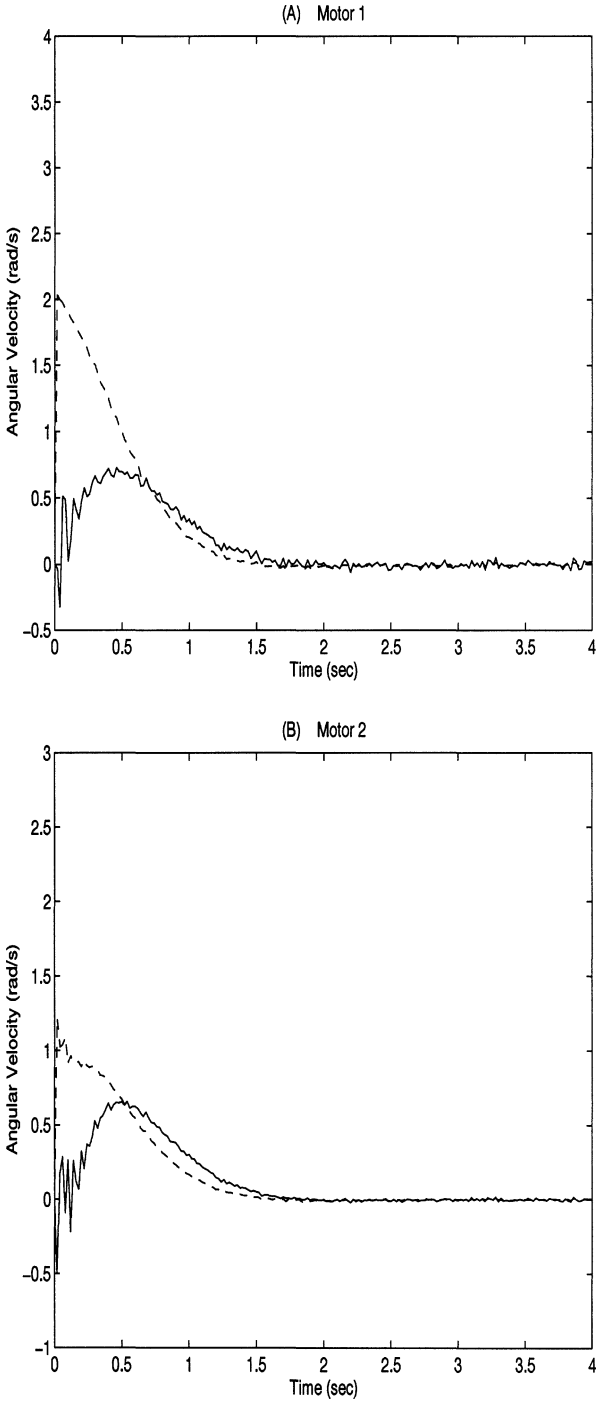

Figure 15. Motor's angular velocities: — actual, - - - estimate.

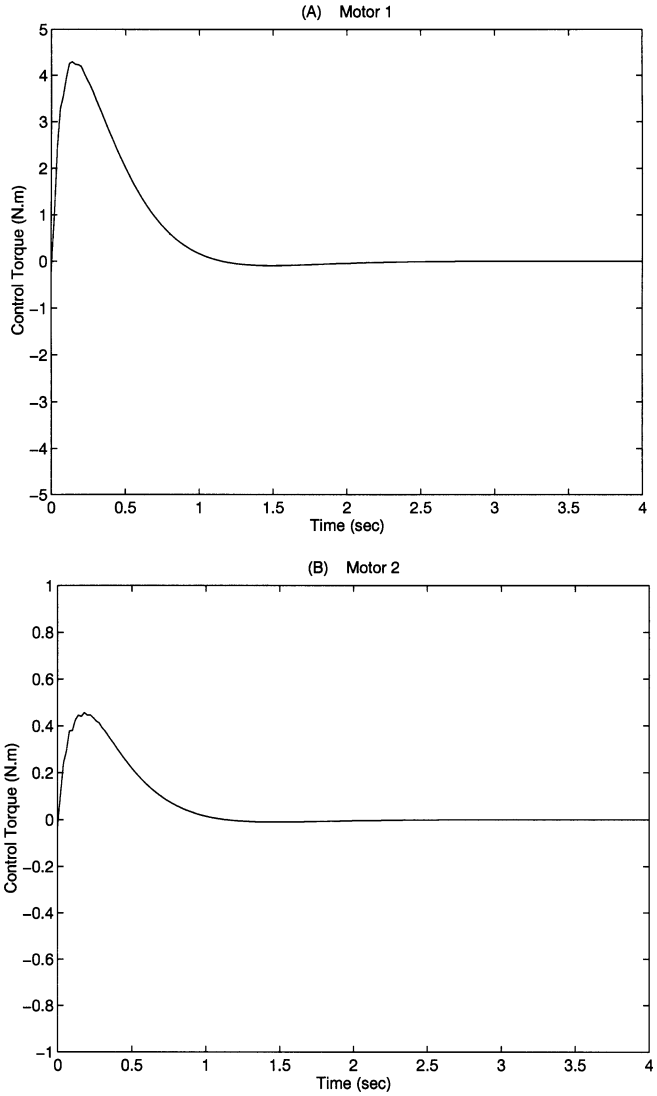

Figure 16. Control input torques.

experimental results indicate the validity of the presented robust controller in controlling the end-point position and force trajectories despite parametric uncertainty in the dynamic model. Future research includes the design and implementation of the control algorithm for two industrial robots (AdeptOne and PUMA 560).

Acknowledgement

The authors wish to acknowledge the support provided by the Institute for Robotic and Intelligent Systems (IRIS) and the Natural Sciences and Engineering Research Council of Canada (NSERC) through research grants to Dr. Hoda A. ELMaraghy.

References

1. Riven, E.: *Mechanical Design of Robots*, McGraw-Hill, New York, 1988.
2. Sweet, L. M. and Good, M. C.: Re-definition of the robot motion control problem: Effects of plant dynamics, drive system, constraints and user requirements, in: *Proc. of 23rd Conf. on Decision and Control*, Las Vegas, NV, December 1984, pp. 724–732.
3. McClamroch, N. H. and Wang, D.: Feedback stabilization and tracking of constrained robots, *IEEE Trans. Automat. Control* **33**(5) (1988), 419–426.
4. Mills, J. K. and Goldenberg, A. A.: Force and position control of manipulators during constrained motion tasks, *IEEE Trans. Robotics Automat.* **5**(1) (1989), 30–46.
5. Yoshikawa, T.: Dynamic hybrid position force control of robot manipulators, description of hand constraints and calculation of joint driving forces, *J. Robotics Automat.* **3**(5) (1987), 386–392.
6. Yoshikawa, T.: Dynamic hybrid position force control of robot manipulators – controller design and experiment, *J. Robotics Automat.* **4**(6) (1988), 699–705.
7. Khatib, O.: A unified approach for motion and force control of robot manipulators: The operational space formulation, *J. Robotics Automat.* **3**(1) (1987), 43–53.
8. De Luca, A., Manes, C., and Nicolo, F.: A task space decoupling approach to hybrid control of manipulators, in: *2nd Internat. Federation of Automatic Control (IFAC) Symposium on Robot Control*, Karlsruhe, Germany, October 1988, pp. 54.1–54.6.
9. Chian, B. C. and Shahinpoor, M.: The effects of joint and link flexibilities on the dynamic stability of force controlled robot manipulators, in: *Proc. of the IEEE Conf. on Robotics and Automation*, Scottdale, AZ, May 1989, pp. 398–403.
10. Eppinger, S. D. and Seering, W. P.: Three dynamic problems in robot force control, in: *Proc. of the IEEE Conf. on Robotics and Automation*, Scottsdale, AZ, May 1989, pp. 392–397.
11. Krishnan, H. and McClamroch, N. H.: A new approach to position and contact force regulation in constrained robot systems, in: *Proc. of IEEE Conf. on Robotics and Automation*, Cincinnati, OH, May 1990, pp. 1344–1349.
12. Mills, J. K.: Control of robot manipulators with flexible joints during constrained motion task execution, in: *Proc. of the 28th Conf. on Decision and Control*, Tampa, FL, December 1989, pp. 1676–1681.
13. Spong, M.: On the force control problem of flexible joints manipulators, *IEEE Trans. Automat. Control* **34**(1) (1989), 107–111.
14. Jankowski, K. P. and ElMaraghy, H. A.: Dynamic decoupling for hybrid control of rigid-flexible-joint robots, *IEEE Trans. Robotics Automat.* **8**(5) (1992), 519–533.
15. Ghorble, F., Hung, J. Y., and Spong, M. W.: Adaptive control of flexible joint manipulators, *IEEE Control System Magazine*, December 1989, pp. 9–13.
16. Hung J. Y.: Robust control design of flexible joint robot manipulator, PhD Thesis, Department of Electrical and Computer Engineering, University of Illinois at Urbana-Champain, Urbana, IL, 1989.
17. Slotine, J.-J. E. and Li, W.: Adaptive strategies in constrained manipulation, in: *Proc. of the IEEE Conf. on Robotics Automation*, Raleigh, NC, March 1987, pp. 595–601.
18. Sira-Ramirez, Hebertt and Spong, M.: Variable structure control of flexible joint manipulators, *IEEE Internat. J. Robotics Automat.* **3**(2) (1988), 57–64.
19. Mrad, F. T. and Ahmad, S.: Adaptive control of flexible joint robot using position and velocity feedback, *Internat. J. Control* **55**(5) (1992), 1255–1277.
20. ElMaraghy, H. A. and Massoud, Atef T.: Adaptive dynamic hybrid position and force control of flexible joint robot manipulators, in: *The 3rd Internat. Sympos. on Experimental Robotics*, Kyoto, Japan, October 1993, pp. 59–67.
21. Isidori, A.: *Nonlinear Control Systems*, Springer, London, 1995.
22. Maciejowski, J. M.: *Multivariable Feedback Design*, Addison-Wesley, Reading, MA, 1996.

23. Spong, M.: Modeling and control of elastic joint robots, *ASME J. Dynamic Systems Meas. Control* **109**(4) (1987), 310–319.
24. Spong, M. W. and Vidyasagar, M.: *Robot Dynamics and Control*, Wiley, New York, 1989.
25. Jazwinski, A. H.: *Stochastic Process and Filtering Theory*, Academic Press, New York, 1970.
26. Massoud, Atef T. and ElMaraghy, H. A.: Design, dynamics, and identification of a flexible joint robot manipulator, *The IASTED Internat. Conf. on Robotics and Manufacturing*, Oxford, England, September 1993, pp. 72–75.